frontiers | Frontiers in Astronomy and Space Sciences

TYPE Original Research
PUBLISHED 19 September 2025
DOI 10.3389/fspas.2025.1652705

OPEN ACCESS

EDITED BY
Denny Oliveira,
University of Maryland, Baltimore County,
United States

REVIEWED BY
Lauri Holappa,
University of Oulu, Finland
Jiaojiao Zhang,
Chinese Academy of Sciences (CAS), China

*CORRESPONDENCE
Chigomezyo M. Ngwira,
chigomezyo.ngwira@nasa.gov

RECEIVED 24 June 2025
ACCEPTED 27 August 2025
PUBLISHED 19 September 2025

CITATION
Ngwira CM, Nishimura Y, Weygand JM, Landwer LJ, Bush DC, Foster JC and Erickson PJ (2025) Evaluating the geomagnetic response to the May 2024 super storm – observations and interpretations. *Front. Astron. Space Sci.* 12:1652705. doi: 10.3389/fspas.2025.1652705

Evaluating the geomagnetic response to the May 2024 super storm – observations and interpretations

Chigomezyo M. Ngwira[1,2]*, Yukitoshi Nishimura[3], James M. Weygand[4], Lois J. Landwer[5,6], Daniel C. Bush[7], John C. Foster[8] and Philip J. Erickson[8]

[1]Space Weather Laboratory, NASA Goddard Space Flight Center, Greenbelt, MD, United States, [2]Department of Physics, The Catholic University of America, Washington, DC, United States, [3]Department of Electrical and Computer Engineering and Center for Space Physics, Boston University, Boston, MA, United States, [4]Department of Earth, Planetary, and Space Sciences, University of California Los Angeles, CA, United States, [5]Cooperative Institute for Research in Environmental Sciences, University of Colorado, Boulder, CO, United States, [6]National Oceanic and Atmospheric Administration Space Weather Prediction Center, Boulder, CO, United States, [7]Missouri Skies Observatory, Albany, MO, United States, [8]Haystack Observatory, Massachusetts Institute of Technology, Westford, MA, United States

On 10 May 2024, a series of coronal mass ejections were detected at Earth followed by one of the most powerful geomagnetic storms since November 2003. Leveraging a multi–technique approach, this paper provides an account of the ground geomagnetic response during the 10–11 May 2024 extreme geomagnetic storm. More specifically, we show that at the mid-latitudes in the American sector, the storm produced extreme ground geomagnetic field perturbations between 01:50 UT and 02:30 UT on 11 May. Then using the Spherical Elementary Current System method, it is shown that the perturbations were associated with an intense westward propagating auroral westward electrojet current. Finally, with the aid of auroral all-sky images from the Missouri Skies Observatory, we demonstrate that an intense isolated substorm event with onset located between the Great Lakes region and the East Coast United States was the main source of the extreme westward electrojet current and the geomagnetic field perturbations at these typical mid-latitude locations. This study emphasizes the increased risk associated with expansion of the auroral oval into the mid-latitudes during extreme geomagnetic activity.

KEYWORDS

space weather, geomagnetic storms, Gannon storm, extreme mid-latitude geomagnetic perturbations, isolated substorm, auroral equatorward expansion

1 Introduction

Space weather is the leading cause of geomagnetic disturbances (GMDs) produced in the near–Earth geomagnetic environment. Large variations in the geomagnetic field created during major GMDs induce electric fields on the surface of the Earth that then elevate the levels of geomagnetically induced currents (GICs) in grounded infrastructure such as electrical power grids, oil or gas pipelines, and navigation and communication

systems (Pirjola, 2000; Pulkkinen et al., 2017). This is of critical concern especially during extreme geomagnetic storm events. For instance, GICs have been known to cause blackouts due to failure of electrical power systems (Wik et al., 2009; Boteler, 2019) and to cause damage to equipment, such as high-voltage transformers, in a waste case scenario (North American Electric Reliability Corporation, 1989; Gaunt and Coetzee, 2007).

Extreme GMDs are rare yet can have a detrimental impact on human–made technology. The limited number of extreme events available for study is a major challenge to understanding the solar wind-magnetosphere-ionosphere coupling dynamics under extreme driving conditions. This is because improving our knowledge of the Earth's geomagnetic environment is key to mitigating the impact of space weather on technology. Due to this growing concern of the potential GIC impact on ground-based technologies, there has been an increasing number of studies to understand the GIC characteristics, the drivers, and the impact on systems (Pulkkinen et al., 2012; Ngwira et al., 2013, 2015; Pulkkinen et al., 2017; Wei et al., 2021; Zou et al., 2022; Weygand et al., 2023; Engebretson et al., 2024; Waghule et al., 2024; Opgenoorth et al., 2024; Ngwira et al., 2025).

Wei et al. (2021) used a multipoint technique that combined space-borne observations with ground geomagnetic field recordings to investigate the characteristic response of the magnetosphere-ionosphere and ground system during the 7 January 2015 storm. Based on the observations, they proposed that localized substorm currents that mapped to conjugate regions of intense geomagnetic field variations, dB/dt, on the ground were driven by multiple bursty bulk flows (BBFs) in the inner magnetosphere. This is consistent with other recent studies showing that BBF-related substorms can produce intense localized geomagnetic perturbations (Sorathia et al., 2023; Waghule et al., 2024; Engebretson et al., 2024; Ngwira et al., 2025). More recently, Milan et al. (2024) linked multiple intensifications convection states to the occurrence of intense dB/dt ("spikes") on the dawnside. The results from Milan et al. (2024) are similar to the work of Sorathia et al. (2023) that related BBFs to the dawnside current wedge (DCW) that is easily distinguishable from the typical substorm current wedge (SCW). Formation of the DCW is linked to the dawn-dusk ring current asymmetry during storms. Clearly, different current systems are attributed to the development of intense GICs during distinct geomagnetic activity at specific local times. Within the auroral zone, intense GICs are commonly associated with auroral features, such as the poleward boundary intensifications, poleward expanding auroral bulges, auroral streamers, omega bands, and pulsating auroras (Ngwira et al., 2018; Zou et al., 2022; Milan et al., 2023; Sorathia et al., 2023).

More recently, Opgenoorth et al. (2024) conducted a comprehensive review of the near-earth geomagnetic environment that highlights the progress and gaps in understanding, prediction, and impacts of GICs with a focus on enhancing understanding of the GMD characteristics vital for GICs, the production of earth conductivity models, the determination of geoelectric fields, and the modeling of GICs in different systems. That report demonstrates that enormous progress has been achieved over the last two decades in understanding the solar wind-magnetosphere-ionosphere dynamics and the impacts of these coupled domains on human technologies on the surface of the Earth. However, there are also many challenges that remain in our ability to more accurately quantify solar wind driving, magnetosphere-ionosphere-thermosphere (MIT) coupling, and the impacts on specific technologies. This is particularly more pronounced during extreme geomagnetic storm events.

On 10 May 2024, a series of coronal mass ejections (CMEs) were detected at Earth followed by one of the most powerful geomagnetic storms since November 2003. This storm stands as the most powerful event in the current solar cycle 25 at the time of this writing. As a result, this event has received wide attention as evidenced by the collection of reports, for example, (Gonzalez-Esparza et al., 2024; Tulasi Ram et al., 2024; Foster et al., 2024; Piersanti et al., 2025; Zhang et al., 2025; Zou et al., 2025; Hayakawa et al., 2025; Waghule and Knipp, 2025). A recent investigation by Tulasi Ram et al. (2024) shows that the dayside magnetopause was significantly compressed within the geostationary orbit at 6.6 RE for around 5.5-h, continuously driven by elevated solar wind dynamic pressure. Those authors also reveal that the geomagnetic storms was a result of two interplanetary CMEs (ICMEs) arriving at Earth separated by about 5-hours.

The present paper provides an account of the near–Earth geomagnetic environment response during recent 10–11 May 2024 extreme geomagnetic storm, hereafter referred to as the "Gannon storm". More specifically, the study is focused on the extreme geomagnetic field variations observed in the American sector during the period between 01:50 UT and 02:30 UT on 11 May. We provide new insight on the extreme geomagnetic perturbations and the related magnetosphere-ionosphere electrodynamics. This report is organized as follows: The data and methodology are outlined in Section 2, while in Section 3 we describe the solar drivers and magnetosphere response. The key observations and interpretations are outlined in Sections 4. Finally, a summary and conclusions are presented in Section 5.

2 Data and methods

2.1 Ground magnetometers

The geomagnetic field observations presented in this study were obtained from SuperMAG, a global network comprising of around 600 ground-based magnetometers (Gjerloev, 2009). The SuperMAG data is processed using a uniform data processing technique and made available to the public. For this study, we leverage existing tools and methods, e.g. (Ngwira et al., 2023, 2025), to perform a routine quality check of the geomagnetic field measurements to ensure the extreme perturbations ("spikes") were not due to artifacts in the data. Details of the ground magnetometer stations that have been used in this study are displayed in Table 1.

2.2 Equivalent ionospheric currents and current amplitudes

For this study, the Spherical Elementary Current System (SECS) method was adopted to compute the ionospheric currents. In the SECS technique, a two-dimensional picture of the ionospheric currents can be derived with an array of well-spaced ground

TABLE 1 The list of ground magnetometer sites used in the analysis presented in this paper. The AACGM coordinate system based on the IGRF 2010 model was adopted for the geomagnetic latitude and longitude. LT represents the local time at each station.

Name	Code	Geo. Lat. [Deg.]	Geo. Lon. [Deg.]	MLAT [Deg.]	MLON [Deg.]	LT [Hours]
High latitudes						
Nain	NAN	56.40	298.30	63.90	22.81	UT – 4.11
Sanikiluaq	T31	56.50	280.80	66.31	−1.92	UT – 5.28
Rabbit Lake	RAL	58.22	256.32	67.00	−40.08	UT – 6.91
Kenia College	T55	60.55	208.74	60.35	−94.22	UT – 10.08
Higher middle latitudes						
Saint Johns	STJ	47.60	307.32	52.60	31.64	UT – 3.51
Ottawa	OTT	45.40	284.45	54.98	2.52	UT – 5.04
Hennepin	R03	44.90	266.27	54.85	−23.71	UT – 6.25
Victoria	VIC	48.52	236.58	53.62	−62.05	UT – 8.23
Middle latitudes						
Fredericksburg	FRD	38.20	282.63	48.05	−0.64	UT – 5.15
Bluesky	R05	41.58	275.83	51.82	−9.99	UT – 5.61
Missouri	R01	38.90	267.78	48.96	−21.37	UT – 6.14
Boulder	BOU	40.14	254.76	48.52	−38.69	UT – 7.02
Fresno	FRN	37.09	240.28	42.63	−54.89	UT – 7.98

magnetometers (Amm, 1997; Amm et al., 2002; Weygand et al., 2012). The method has regularly been applied to calculate the equivalent ionospheric currents (EICs), which are parallel to Earth's surface, and the spherical elementary current (SEC) amplitudes, which are a proxy for the field-aligned-currents (FACs). In general, the EICs are calculated from a matrix inversion of the ground magnetic disturbances. One of the important features of this technique is that it requires no integration time of the magnetometer data. There are two outputs from the SECS inversion. The first output is the EICs, which are a combination of the real Hall and Pedersen currents. The temporal and spatial resolutions of the EICs are 10 s, and 6.9° geographic longitude (GLong) by 2.9° geographic latitude (GLat), respectively. The second output is the SEC amplitudes, which are a proxy for the field-aligned-like currents, with a 10 s temporal resolution and 3.5° GLong by 1.5° GLat spatial resolution. Both set of currents are derived at an altitude of 100 km. For more details on the SECS method, see the following resources: (Amm, 1997; Weygand et al., 2011, 2012, and references therein).

In the present study, an estimate of the auroral oval equatorward boundary location is performed using the SECS technique outlined by Weygand et al. (2023). In that paper the equatorward boundary location was fitted visually by selecting points along a contour of about 0.5 μAmp/m^2. However, the equatorward boundary for the Gannon storm was frequently below the preset SECS grid for calculating the currents. Therefore, to get a good fit, a rough boundary was selected not at the typical 0.5 μAmp/m^2 value used in previous studies. It must be noted that in the present case, getting a fit was difficult because currents were mostly in disarray due to the extreme nature of the storm. But one of the challenges to extending the grid further south is the limited number of stations (~3) that might help to obtain a good fit of the boundary location at μAmp/m^2. We refer readers to Weygand et al. (2023) for more details on the auroral boundary estimation process.

2.3 Auroral all-sky images

The Missouri Skies Observatory (40.25 N, 94.32 W, www.missouriskies.org) is an amateur-run facility located within the city limits of rural Albany, Missouri. Its main instrument is a 50 cm reflector telescope. As part of citizen science activities, off-the-shelf surveillance camera equipment mounted on the observatory and other points around the property are used. The all sky cameras (ASCs) are unmodified and have settings tweaked to record, at maximum sensitivity, real-time movies of satellite phenomena, airglow, auroras, and meteors. The ASC field of view is 180°.

Sometimes, the Observatory hosts live streams of important auroral events for the public interest, such as the Gannon storm. During the May 2024 great auroral event, the Observatory recorded color ASC, wide-angle color north-looking, and black and white east-looking video with an exposure time of 1-s and recording frame rate of 1/30-sec. Selected frames from the Missouri Skies ASC video showing the auroral sequence on 11 May are presented in Section 4 of this study.

3 Solar drivers and magnetospheric reaction

3.1 Solar and interplanetary conditions

In May 2024, solar cycle 25 (SC-25) hit a new high when the monthly sunspot number reached 172 beating the previous high of 160 recorded in June/July of 2023. In comparison to the previous two cycles, the maximum monthly sunspot number reported for SC-25 (217, August 2024) is about 67% higher than the 146 recorded for SC-24 in February 2014, while SC-23 had a maximum of 244 in July 2000. Interestingly, during the period 8–9 May 2024, the Sun continuously unleashed several CMEs in quick succession including Earth-directed ones. All CMEs were linked to X-class or strong M-class solar flares dominated by two powerful X-class flares with magnitude X2.25 and X1.12 (Tulasi Ram et al., 2024). Shortly there after on 10–11 May, another set of powerful X-class flares with magnitude X3.9 and X 5.8 were also launched. According to the NOAA Space Weather Prediction Center (SWPC), the solar Active Region AR3664 was the candidate for Earth-directed CMEs.

In general, the observed CMEs had average speeds ranging from 456 km/s to a maximum exceeding 2000 km/s. Given that, it is very likely that later CMEs may have caught up with preceding ones, leading to collisions or merging events (CME cannibalism). This type of interaction can amplify CME speed, plasma density, and magnetic field strength, substantially intensifying the shock strength upon reaching Earth's magnetosphere, which can trigger G5-level GMDs. Unlike other extreme events (e.g., Halloween Storm of 2003), the Gannon Storm's rapid sequence of CMEs led to stronger magnetospheric shocks through CME–CME interactions, thus creating a powerful, long-duration geomagnetic storm. The solar wind and the interplanetary magnetic field (IMF) conditions during the Gannon storm are presented in Figure 1. The data were obtained from the OMNIWeb service available through the NASA/GSFC Space Physics Data Facility provided by CDAWeb (https://omniweb.gsfc.nasa.gov/). The figure contains the IMF magnitude (a), the IMF-By (blue) and Bz (red) components (b), the solar wind density (c) and speed (d), and the geomagnetic field SYM-H index (e), a high-resolution equivalent of the Dst index.

Following the arrival of the first ICME forward shock (CME-1) around 17:05 UT on 10 May (Figure 1), the IMF magnitude (a), speed (c), the density (d), and the dynamic pressure (e), were all observed to suddenly increase, as traditionally expected for most CMEs. It must be noted that the density and speed were slightly elevated before the first CME arrival starting around 15:00 UT, which is also reflected in the SYM-H index in Figure 1f. It is not clear at present what role these elevated levels of density and speed may have played in the subsequent storm dynamics and strength. Nevertheless, this topic related to pre-conditioning of the magnetosphere will not be addressed in the present paper. A second ICME (CME-2) forward shock was detected shortly after 22:00 UT, as also indicated by the second dashed line in Figure 1. In the early phase and main phase of the storm (first 10 h), the IMF-Bz was predominately southward with a peak value around −53 nT. The high IMF-Bz levels and the sustained southward orientation is one of the reasons for the development of an extreme geomagnetic storm, as is well-known.

3.2 Magnetospheric response

On the Earth's surface, the first CME arrival is reported to have produced an extreme sudden commencement (SSC), as recorded by ground magnetometers (Piersanti et al., 2025). A comparison of the Gannon storm features to other historical extreme events is displayed in Table 2. The SSC perturbation (ΔSSC = peak SSC value−value before CME arrival) in column two of the table is derived from SYM-H index data. In their investigation of the geomagnetic response to the Gannon storm focusing on the European sector, Piersanti et al. (2025) found that the strong solar wind pressure coupled with a large sustained southward IMF-Bz and a favorable shock inclination angle resulted in an extreme SSC with an amplitude of roughly 180 nT recorded in the near–dusk sector at the Grocka (40.55°, MLT = 18:30) ground magnetometer station in Serbia. They attributed this extreme SSC to both ionospheric and magnetosphere drivers. Regarding the timing of the SSC, we note the existence of two different reported arrival times at 16:34 UT and 17:05 UT by Tulasi Ram et al. (2024) and Piersanti et al. (2025), respectively. Based on the currently available level 2 OMNI solar wind and the ground magnetometer data, we adopt 17:05 UT as the arrival time of the CME.

Evidently on the Dst scale, the Gannon storm is one of the most powerful geomagnetic storms of recent times ranking as the third largest storm in modern history (1985–2024) following the March 1989 and November 2003 extreme events, as illustrated in Table 2. With a recorded peak negative excursion of the Dst index at 406 nT according to World Data Center Kyoto (https://wdc.kugi.kyoto-u.ac.jp/) equivalent to the SYM-H index reaching about −518 nT, this event stands as the most intense storm of solar cycle 24–25 at the time of this writing. Solar wind energy transferred through multiple channels affected the entire Geospace. Zhang et al. (2025) report of a new proton belt with high energy fluxes was created by the combine effect of inward proton penetration from solar proton events and likely energization due to significant compression of the magnetopause with the southward IMF-Bz during the SSC period. Upon further inspection of the solar wind characteristics listed in Table 2, it is immediately clear that this storm was not extraordinary in its drivers, but rather comparable to other historical events. We must make mention here that the October 2003 storm IMB Bz and density information is estimated due to widely known data challenges experienced during that era.

4 The ground geomagnetic response

From a space weather perspective, the auroral region is well-known to produce the most dramatic geomagnetic activity during

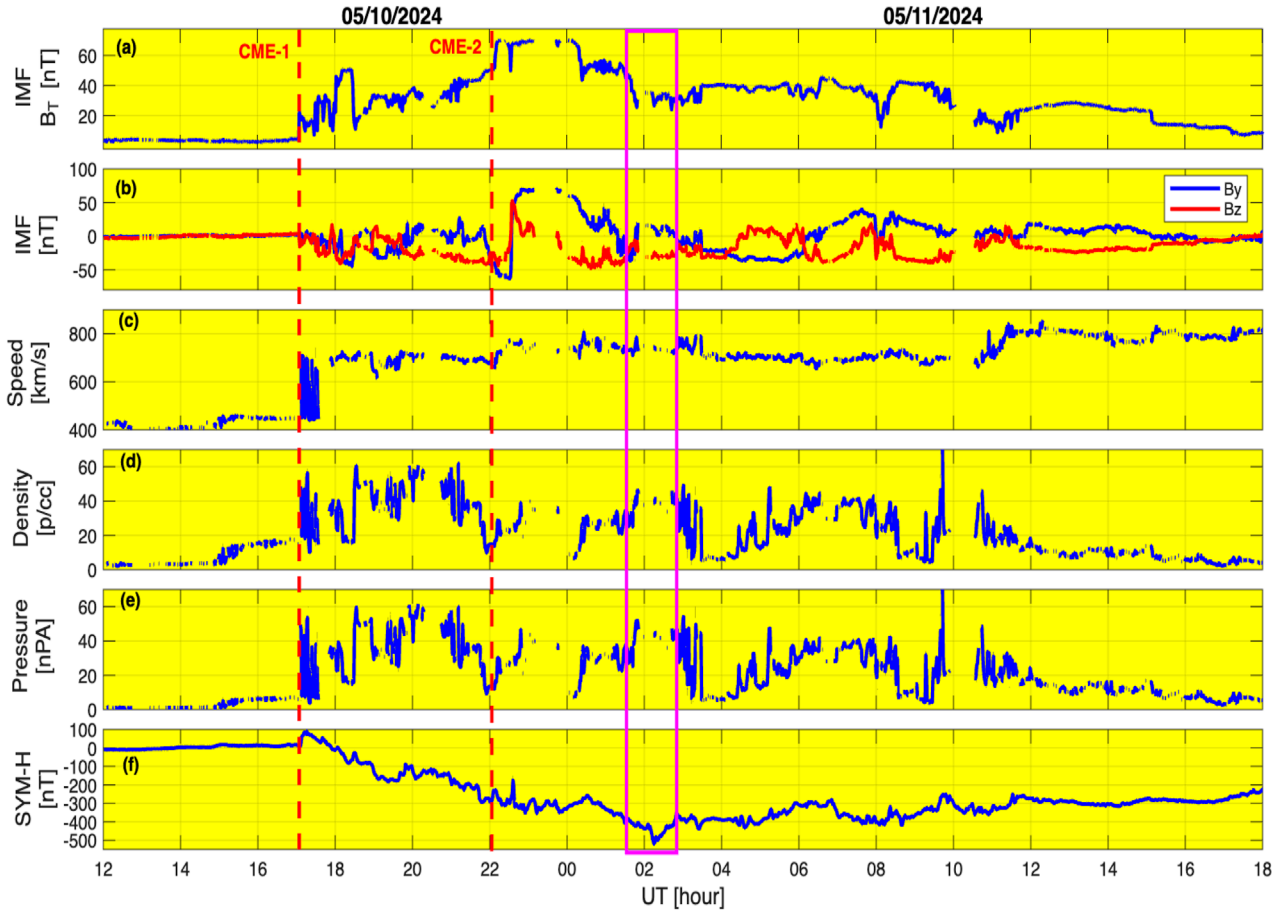

FIGURE 1
The OMNI solar wind and IMF conditions during the Gannon storm. Panels show: **(a)** IMF magnitude (|B|), **(b)** IMF By (blue) and Bz (red), **(c)** solar wind speed, **(d)** proton density, **(e)** dynamic pressure, and **(f)** the geomagnetic field SYM-H index. The two red dashed lines indicate the CME arrivals, while the magenta rectangle marks the period of interest in the present study.

TABLE 2 Comparison of Gannon storm to other historical geomagnetic storms in the last 40 years. Displayed in the table are the date of storm, the SSC perturbation (ΔSSC = peak SSC value−value before CME arrival), maximum Dst index value, time of Dst maximum, peak IMF-Bz, peak speed, and peak density. Note that the peak IMF-Bz, speed, and density reflect conditions before the peak Dst instance. Only storms with a Dst value below −350 nT are listed in order of the storm strengthen. The Gannon storm is highlighted in blue color.

Date	ΔSSC	ΔSSC time	Max Dst	Peak IMF-Bz	Peak speed	Peak density
	[nT]	[UT]	[nT]	[nT]	[km/s]	[n/cc]
Nov 2004	89	19:20	−374	−50	756	62
Oct 2003	87	06:14	−383	−58	~1800+	~30–40
May 2024	78	17:15	−406	−53	789	63
Nov 2003	48	08:06	−422	−52	755	28
Mar 1989	54	01:31	−589	−200	960	60

both geomagnetic storms and quiet times. This is largely attributed to the intense current systems that connect this region to the magnetosphere and solar wind domains. To investigate the auroral response during the Gannon storm, we begin by comparing this storm to other historical extreme events using the SuperMAG SML index displayed in Figure 2. The figure contains the SML values for all the five superstorms (color coded) listed in Table 2. Clearly, there are a number of extreme westward electrojet signatures with SML less than −2500 nT, a level considered to represent supersubstorms (Tsurutani et al., 2015; Hajra et al., 2016). According to earlier

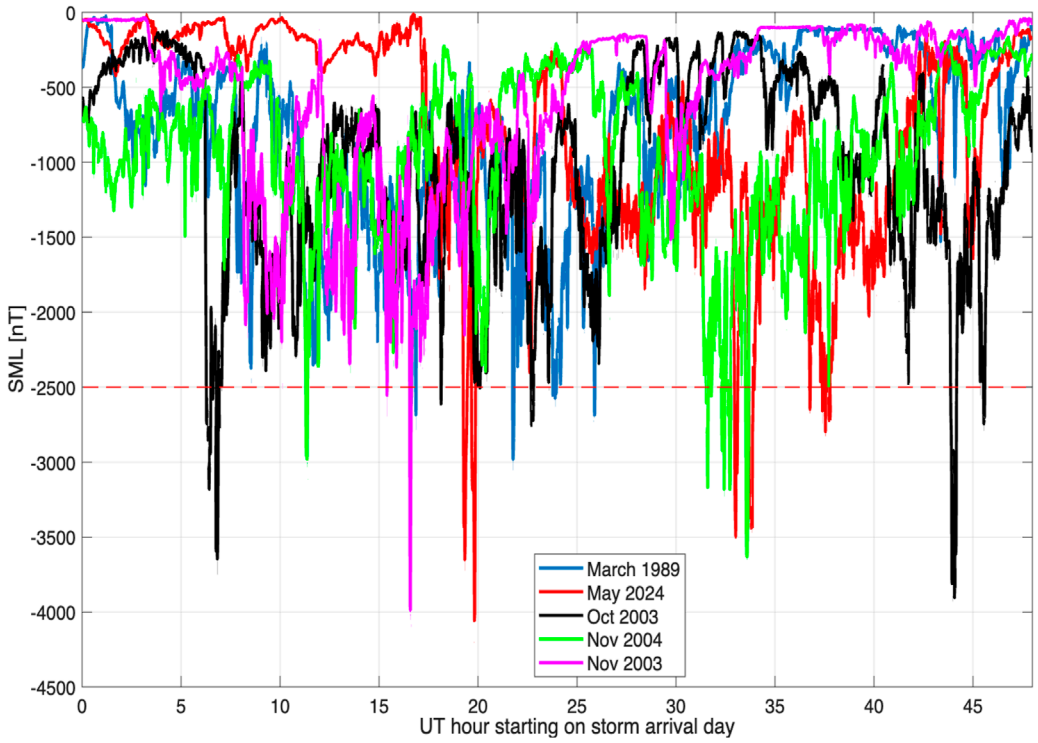

FIGURE 2
Comparison of the SuperMAG SML index for the superstorms listed in Table 2. Colored lines represent different storm dates: March 1989 (blue), May 2024 (red), October 2003 (black), November 2004 (green), and November 2003 (magenta). The red dotted line indicates the level considered for supersubstorm classification. The time interval shown covers a period of 2 days starting on the day of the associated CME arrived for each event, respectively.

works, supersubstorms are considered to be distinct SML peaks separated by >6 h in preference to repetitive index fluctuations (Zou et al., 2025). On average, these explosive events have low occurrence frequency with only a few limited observations per year (Hajra et al., 2016). Additionally, prior studies suggest that supersubstorms occur mostly during the geomagnetic storms main phase with some spotty observations during recovery phase and non-storm times (Hajra et al., 2016; Zou et al., 2025).

A closer inspection of Figure 2 shows that the Gannon storm of May 2024 (red) produced significantly large geomagnetic deviations in the auroral zone comparable to other historical storms. More specifically, even though there are six times when SML was <-2500 nT during this event, only two of those intervals can be consider as supersubstorm signatures based on the definition outlined above. In a recent report, Zou et al. (2025) investigated the supersubstorm signatures on 10 May at 19:19 UT and 19:49 UT during the main phase, while the other event occurred in the recovery phase on 11 May at 09:00 UT and 09:48 UT. They concluded that the first event was a typical substorm in nature, whereas the second event was related to enhancement of general magnetospheric convection following a solar wind pressure increase.

In addition to the supersubstorm signatures emphasized above, we have also identified some unique features in the ground geomagnetic field measurements that are now presented and discussed below. In particular, two aspects are emphasized here, which include the extreme geomagnetic field variations observed in the North American sector following an isolated substorm event and the related auroral electrodynamics.

4.1 Extreme mid-latitude geomagnetic perturbations

Here, we focus on the less intense substorm event deep in the main phase of the storm on 11 May. An account by Foster et al. (2024) estimates the onset of this substorm to be between 02:00–02:02 UT (~22 MLT) based on images from the Boston University all-sky imager located at Millstone Hill, Massachusetts (42.6 N, 71.3 W). This puts the location of the onset in the vicinity of the Great Lakes and East Coast region of the United States. Interestingly, the substorm event was not captured on any of the well-known substorm lists. The inability to capture some substorm onsets is a widely documented limitation (Newell and Gjerloev, 2011; Chu et al., 2015; Forsythe et al., 2020; Ohtani and Gjerloev, 2020; Lao et al., 2024), but is outside of the scope of this current report. However, it would suffice to say that the extreme equatorward expansion of the auroral oval at the time of this event could be the main reason why this particular substorm onset was not captured. It should be noted that under extreme equatorward expansion, the stations used in the computation of the electrojet indices may have been located outside of the auroral oval coverage.

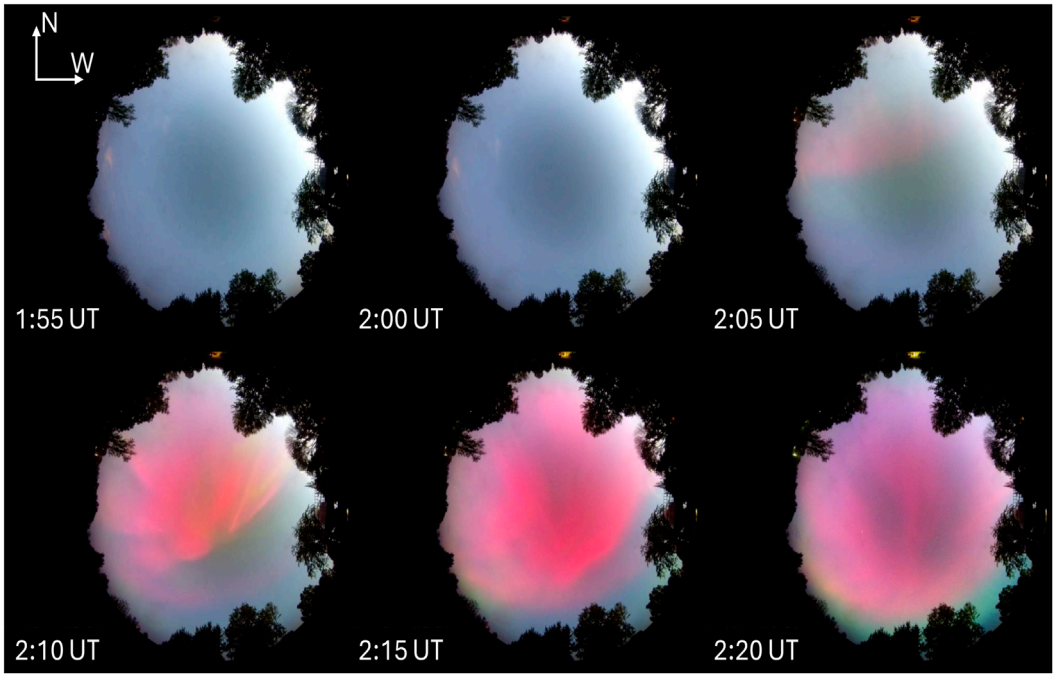

FIGURE 3
Sky view of selected composite images captured at the Missouri Skies Observatory on 11 May 2024. The images display evidence of red aurora moving over the ground location. Note that North is to the top and west is to the right, as indicated by the arrows in the top left corner of the images.

Figure 3 shows a series of ASI images from the Missouri Skies Observatory (40.25N, 94.32W) taken on 11 May 2024. As seen in Figure 3, before 02:00 UT, the images do not show any auroral activity, but red aurora suddenly appears to the north around 02:05 UT. The red aurora is then observed to extend southwestward with time, as revealed in Figure 3. The western edge of the red aurora is the front of the substorm westward expansion, and it includes an auroral streamer. In a recent report, Foster et al. (2024) investigated the changes in ionospheric total electron content (TEC) triggered by the storm-induced energetic particle precipitation during the Gannon storm. They provide a detailed account of the intense auroral breakup and westward surge occurring at the peak of that storm. Foster et al. (2024) also showed that sudden bursts of significantly elevated vTEC were related to the intense red aurora located on the leading edge of the equatorward and westward TEC enhancement. They attributed this TEC increase to extremely low-energy precipitation following the rapid substorm breakup.

In Figure 4 we examine the horizontal geomagnetic field observations on the surface of the Earth. Exhibited in this figure are the geomagnetic field B_x component (top) recorded at selected ground stations and the rate of changes of B_x (bottom) for the period 10–11 May, 2024. Details of these ground sites are listed in Table 1. For this investigation, a chain of mid-latitude magnetometers running from East to West across the continental United States was selected. A closer look at Figure 4 shortly after 02:00 UT reveals a clear substorm characteristic commonly seen in ground magnetometer observations. We note that before the marked decrease in the B_x component, there was a sudden rapid enhancement of the field. This is a typical signature associated with the mid-latitude positive bay (MPB) phenomena, a frequently observed feature driven by auroral substorm–related activity (Chu et al., 2015; McPherron and Chu, 2017). However, it was only recently that Ngwira et al. (2023) showed, for the first time, a direct relation between MPBs and the occurrence of large GICs using data over the North American region. The presence of auroral streamers in the ASI images suggest that the current system driving the geomagnetic perturbations involves BBFs in the magnetosphere (Lyons et al., 2013). Streamers are considered to extend equatorward within the auroral oval from PBIs, which have been linked to flow bursts (BBFs) that can transport plasma across the nightside magnetic separatrix into the plasma sheet (Lyons et al., 2011) and are therefore related to localized regions of enhanced tail reconnection. While streamers can occur during many different geomagnetic conditions, they are commonly seen as localized structures during the much larger-scale auroral displays of a substorm expansion phase (Henderson et al., 1998).

What is more captivating about this event in Figure 4 is the level of perturbation observed at these mid-latitude locations. Firstly, before the negative excursion, there was a sharp increase of B_x from −316 nT to −175 nT (ΔB_x = −141 nT) at the USGS Fredericksburg (FRD) Observatory in Virginia and an extreme increase from −307 nT to 142 nT (ΔB_x = −449 nT) at Missouri magnetometer site (R01). The sharp enhancement was quickly followed by rapid decrease with an absolute value of the geomagnetic perturbation, ΔB, roughly ~641 nT recorded at FRD and ~733 nT at R01. These levels of change are extremely large and rare for these mid-latitude locations. In the American sector, Figure 1 of Foster et al. (2024) also reported very rare magnetometer deviations of −700 nT (Missouri) to −1000 nT (Millstone Hill) using the MagStar observation network. In addition, Waghule and Knipp (2025) presented the temporal

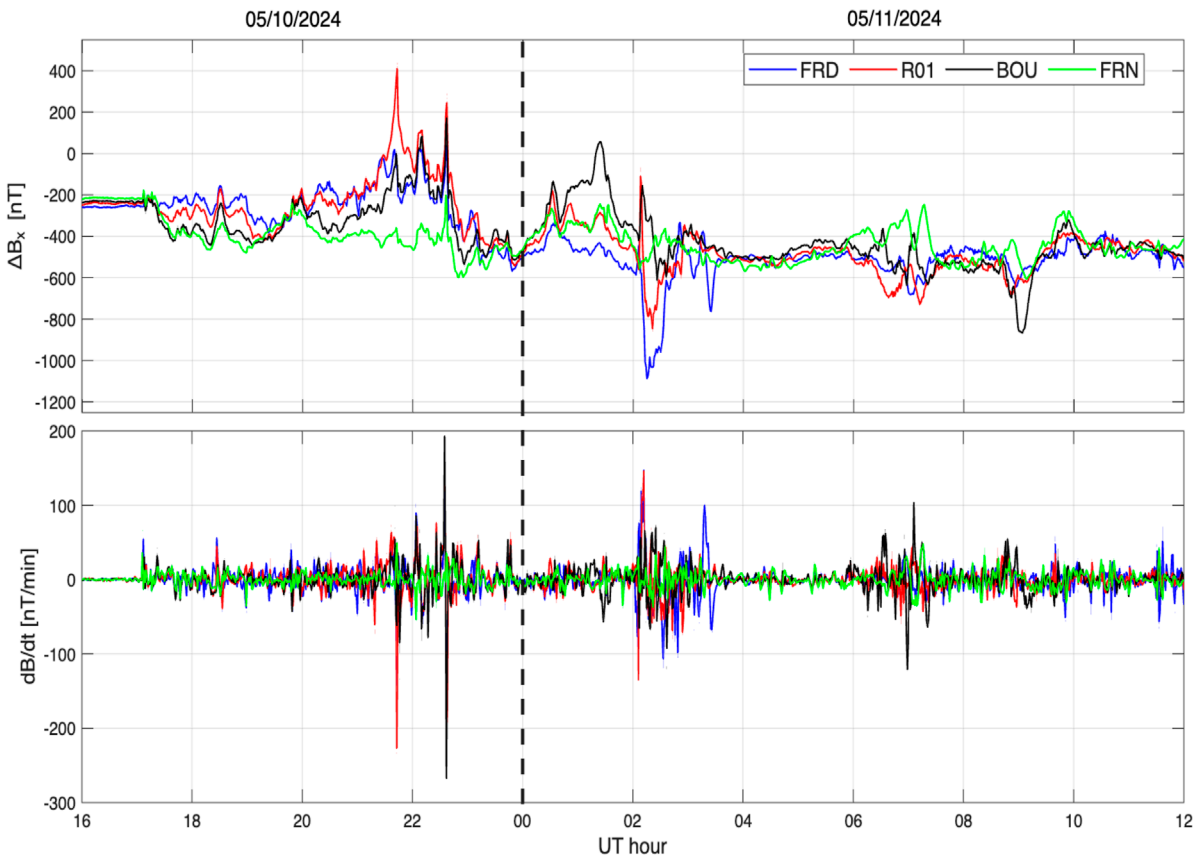

FIGURE 4
Top: The horizontal geomagnetic field B_x component variations recorded at mid-latitudes of the United States on 10–11 May 2024. The panel shows variations in ΔB_x for FRD, R01, BOU, and FRN, marked in blue, red, black, and green respectively. The geomagnetic field rates of change are shown in the bottom panel. The traces are color coded according to the legend in the top panel. The vertical black dashed line indicates the separation between the 2 days investigated in the present paper.

correlation of large GICs recorded near Fredericksburg, Virginia, and the ionospheric observations derived from GNSS TEC and Radars from the SuperDARN network in the United States. Their investigation suggests that peak GIC variability occurred deep in the main phase of the storm, during which time, the F-region ionosphere appears to have been significantly elevated and expanded. The present study and other cases from previous studies highlight the complexity and severity of the Gannon storm event.

Notably, the storm's impact on the ΔB perturbations was observed to propagate westward accompanied by a reduction in the intensity, as seen from Figure 4 for FRD, R01, BOU, and FRN. This westward propagation is consistent with the initiation of the auroral electrojet (AEJ) enhancement reported by Foster et al. (2024). According to Foster et al. (2024), the auroral intensification extended westward through the central United States near 94 W longitude around 02:02 UT, while there was a large expansion and southwestward propagation associated with auroral breakup that appeared near 02:05 UT (~21 MLT). Interestingly, these intense perturbations revealed here were confined to certain portions of the North American sector in the vicinity of the substorm onset region around the Great Lakes and East Coast of the United States. This strongly suggests that the impact of the substorm was both spatially and temporally localized in nature. It is also important to note that, similar substorm-related perturbations in ground geomagnetic field data were also seen in the South American sector (not shown).

In contrast to the mid-latitudes (Figure 4), the geomagnetic field characteristics at high-latitudes and the higher mid-latitudes are presented in Figure 5. Firstly, the geomagnetic response at the high-latitudes and the higher mid-latitudes are vastly different. For instance, we clearly see large perturbations at higher mid-latitudes around 02:00 UT on 11 May, whereas some high-latitude stations only show perturbations at 30-min before 02:00 UT. As well, the signature of the supersubstorm on 10 May is more visible at high-latitudes than the mid-latitudes. However, the most notable differences are observed during the recovery phase when significantly large perturbations are captured over the high-latitudes. These perturbations are accompanied by equally large fluctuations in the field, dB_x/dt, that correspond to the intervals when SML index was < -2500 nT, as demonstrated in Figure 2.

4.2 Auroral currents and dynamics

Turning our attention to the auroral currents and the boundary dynamics, we utilize the EIC and current amplitude maps derived

FIGURE 5
The horizontal geomagnetic field B_x component variations recorded at high-latitudes **(a)** and higher mid-latitudes **(c)** of the North America on 10–11 May 2024. Their respective rates of change are shown in panels **(b)** and **(d)**. The traces are color coded according to the legends provided.

from the SECS technique outlined earlier. Figure 6 shows a series of SECS maps for this event in the interval between 01:55 UT to 02:15 UT on 11 May. As noted before and seen in Figure 2, this interval does not contain any supersubstorms, however, the isolated intense substorm event during the said period caused extreme geomagnetic field deviations at mid-latitudes in the American Sector, as discussed previously.

Thorough examination of Figure 6 shows that before 02:00 UT the EIC was weak (small arrows) over most of the Continental United States, except to the North Western region, while a clear two cell convention pattern existed to the north in Canada and the Arctic region. The top panel (a) shows orange squares for the high-Latitudes, orange circles for higher mid-latitudes, and orange triangles marking mid-latitudes. The Missouri Skies observatory is represented by a mauve star. At 02:05 UT, a sudden westward intensification of the EIC is observed around the East Coast and Great Lakes region. The intensified current then propagates westward with time. This is consistent with the geomagnetic recordings in Figure 4 showing the ΔB_x perturbation propagating to the west with decreasing intensity. In addition, Foster et al. (2024) reported similar westward propagation during this event based on the observed GPS TEC perturbations over North America. They attributed the observed Large TEC perturbations to the westward expansion of low-energy electron precipitation captured by direct auroral observations.

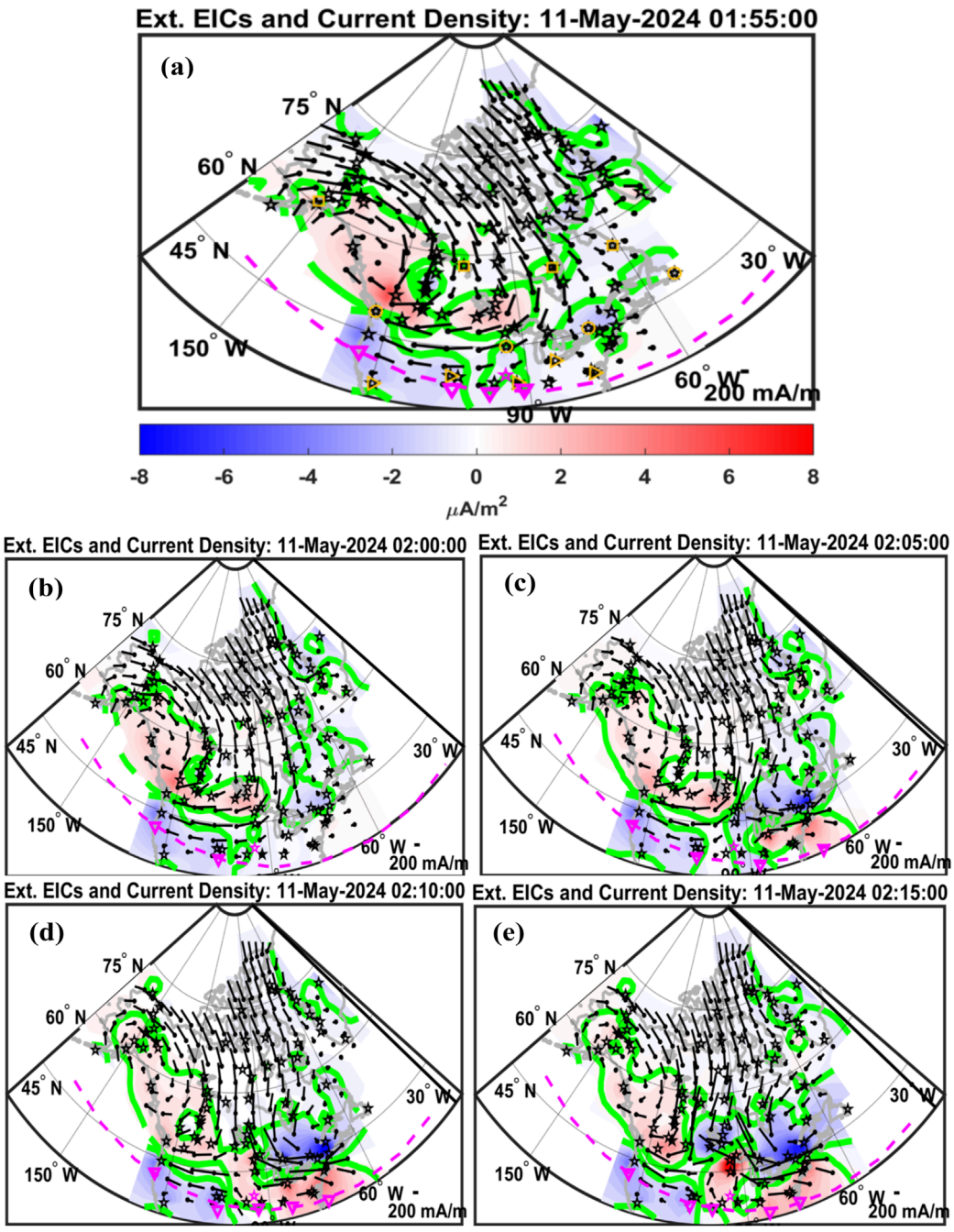

FIGURE 6
SECS maps of horizontal equivalent currents (black vectors without arrow heads originating at grid points denoted by black dots) and vertical current amplitudes (with intensity and sign given in the color bar at the bottom). The panels **(a–e)** are SECS maps starting at 01:55 UT to 02:15 UT on 11 May, 2024. In the top panel **(a)**, the orange squares mark the high-Latitudes, orange circles higher mid-latitudes, and the orange triangles mark the mid-latitudes. Missouri Skies observatory is marked with a mauve star. The dashed mauve curve is the estimated equatorward boundary location. The green curves show boundaries of the upward and downward currents, while the black solid line denotes geographic midnight. The geographic coordinate system is used.

Furthermore, a careful look at the EIC currents in Figure 6 indicates that the strongest geomagnetic perturbations are in the region between the upward (red) and downward (blue) current systems. According to literature, this is the region with the most intense auroral currents, as discussed in previous reports (Ngwira et al., 2018, 2023; Engebretson et al., 2024). Another interesting features is the formation of the Harang (red) upward current system between 02:00 UT to 02:10 UT on 11 May. The Harang reversal (HR), sometimes known as the Harang discontinuity, is a longitudinally extended ionospheric signature near midnight where electric fields and plasma flows reverse direction from westward to eastward with decreasing latitude

(Harang, 1946; Erickson et al., 1991). It is well understood that the HR poleward extension maps to the plasmasheet, while its equatorward extension maps close to the inner edge of the plasmasheet (Erickson et al., 1991). In the magnetic midnight sector where the HR region maps to the magnetotail, the reversal is viewed as a fault line isolating the inflated and collapsed magnetic fields during substorms (Maynard, 1974), whereas some studies suggest that substorm injection occurs in the vicinity of the HR (Weygand et al., 2008; Despirak et al., 2022).

In a study on the coupling between the HR evolution and substorm dynamics using a combination of SuperDARN, DMSP, and IMAGE observations, Zou et al. (2009) found that the substorm auroral onset appeared quite near the center of the HR flow shear, which they considered to be related to the development of the substorm upward FACs. The location and characteristics of the HR are controlled by the IMF orientation, including the IMF clock angle. Fundamentally, the IMF clock angle, specifically the IMF-By, can determine the dynamics and properties of the HR by modulating the ionospheric convection pattern, magnetotail configuration, and AEJ strength and distribution (Anderson et al., 2008; Grocott et al., 2010). Therefore, the HR appearance reflects enhanced magnetospheric plasma convection in the magnetotail that involves an upward flowing FACs from the ionosphere due to diamagnetic ion drift. Its latitudinal location is associated with the strength of geomagnetic activity, often propagating equatorward as the intensity of activity increases, as established in Figure 6. Whereas the southward IMF-Bz is considered a primary condition for the development of GMDs, IMF-By also plays a major role, particularly it strongly influences the dawn-dusk asymmetry (Yoshizawa, 1986; Ohtani et al., 2018).

The dependence of GMDs on the orientation of the IMF-By component has continued to receive wide attention (Holappa et al., 2021; Engebretson et al., 2022; Ohtani et al., 2023). During the Gannon storm, there were two particularly interesting intervals when IMF-By experienced sharp reversals going from negative to positive orientation. At the time of the first flip on 10 May, IMF-By changed from around −64 nT at 22:27 UT to 69 nT at 22:48 UT. The dramatic IMF-By flip happened simultaneously with the IMF-Bz sudden rotation from about −40 nT to 50 nT under high solar wind velocity (~770 km/s) and strong dynamic pressure around 30 nPa, as illustrated in Figure 1. The unique geomagnetic response to this flip has been reported in recent papers (Kleimenova et al., 2025; Vichare and Bagiya, 2024; Ohtani et al., 2025). We see in the present study (Figures 4, 5) that this extraordinary IMF-By flip was also associated with some intense geomagnetic perturbations at mid-latitudes with dB/dt exceeding an absolute value of ~260 nT/min. This level of perturbation is not common at these latitudes during most storms, but appears largely in association with more severe events, such as the Gannon storm.

In contrast, the second IMF-By flip on 11 May turning from −26 nT at ~01:44 UT to 12 nT 2-min later at 01:46 UT has not been reported in previous studies, to our knowledge. During this same period, the IMF-Bz become strongly southward ranging between −8 nT and −32 nT. The formation of the HR in Figure 6 matches up pretty well with the rotation of the IMF-By component near 02:00 UT. Note that prior to about 02:00 UT there is no upward current (red) at Missouri Skies Observatory. However, at 02:05 there is a little bit of red aurora (Figure 3) and the spherical elementary current (Figure 6) shows some upward current but to the east. At 02:10 UT there is upward current (probably the strongest upward current in that region between 01:30 to 02:30 UT) at Missouri Skies Observatory, which is associated with discrete auroral streamer at the observatory (Figure 3). In the all-sky images at 02:15 UT and 02:20 UT there still is strong red aurora and upward current around Missouri Skies Observatory. Figure 1 illustrates that after the second flip around 01:45 UT, the IMF-By remained predominately positive for almost 1-h. At the typical mid-latitudes (Figure 4), the dB/dt were large during the IMF-By flip on 10 May, however, at the higher mid-latitudes (Figure 5d), the dB/dt were much more intense around 02:00 UT on 11 May. These dB/dts were even larger than those seen at high-latitudes (Figure 5b) during the specific time window. This case highlights the complex nature of the solar wind-magnetosphere-ionosphere coupling process. Furthermore, it must be noted here that no Pi2 pulsations are present (not show) in association with the second IMF rotation. However, Pi2 pulsations were present earlier in the storm main phase in association with the dramatic IMF rotation around 22:30 UT as revealed by Kleimenova et al. (2025).

Finally, we turn our focus to the auroral oval equatorward boundary dynamics. This location is estimated using the SECS technique and is depicted by the dashed mauve curve in Figure 6. Understanding the motion of the boundary is important in terms of the location and magnitude of the geomagnetic effects on the ground. Specifically, the auroral oval moving into regions that are considered less prone to intense auroral currents, e.g., the lower 48 States of the United States. However, it is highly possible that the extent of equatorward boundary may have been much further south than depicted here. There were a number of reported aurora sightings in low latitude regions, including Mexico (Gonzalez-Esparza et al., 2024; Hayakawa et al., 2025). One of the limitations to getting a more accurate location of the boundary is the sparse density of magnetometers over the United States and Mexico, as outlined earlier. Obtaining a boundary is further complicated by the intensity of the Gannon storm, as manifested by the messy current patterns produced in Figure 5. Most of the new USGS variometers are closer to the northern United States boarder and really only two stations contribute to the boundary below 35 deg GLat. Therefore, the majority of the time the boundary could be below the "field of view" of the spherical elementary current grid. In general the equatorward boundary sits between 40 deg and 45 deg MLat at magnetic midnight and possibly lower between 01:30 and 01:45 UT (~42 deg MLat) and higher between 02:15 and 02:30 UT (44 deg MLat). Lastly, we also note that the Fresno (FRN) magnetometer site sits outside of the estimated auroral boundary location, which could explain why the geomagnetic field response signature is much different to the other mid-latitude stations in Figure 4.

5 Summary and conclusion

The powerful geomagnetic storm of May 2024 emphasizes the increased risk associated with expansion of the auroral oval to lower latitudes during extreme geomagnetic activity. While there are a number of prior studies that provided different insights about this storm, the present paper is focused on the ground geomagnetic response at the mid-latitudes in the American sector.

Ground geomagnetic field recordings show that the storm produced extreme perturbations typically not seen at such locations. We see in the present study (Figures 4, 5) that the extraordinary IMF-By flip centered around 22:30 UT on 10 May was associated with some intense geomagnetic perturbations at mid-latitudes with dB/dt exceeding an absolute value of ~260 nT/min. This level of perturbation is rare at these latitudes appearing largely in connection with more severe events, such as the Gannon storm. The largest perturbations were seen near the Great Lakes/East Coast region, whereas the intensity of the perturbations was noted to decrease towards the west over the United States. Using ASI images from the Missouri Skies Observatory, this paper reveals that the extreme geomagnetic perturbations were related to an intense isolated substorm event with an onset location located between the Great Lakes region and the East Coast of the United States.

Furthermore, SECS maps shows the formation of the Harang upward current system whose formation follows the rotation of the IMF-By component. Following this rotation at ~01:45 UT (Figure 1), the IMF-By remained predominately positive for almost 1-h. The dB/dt values at the usual mid-latitudes (Figure 4) were large following the IMF-By flip on 10 May, however, the levels were much more intense at the higher mid-latitudes (Figure 5d) around 02:00 UT on 11 May. During this time period, derived dB/dt values exceeding ~500 nT/min were even larger than those seen at high-latitudes (Figure 5b). This event emphasizes the complex nature of the solar wind-magnetosphere-ionosphere coupling process. In addition, it was observed that the strongest geomagnetic perturbations where in the region between the upward and downward current systems, a region with the most intense auroral currents, as discussed in prior studies. For the Gannon storm, this region was pushed deep into the mid-latitude locations, which is not usual for most storms. Finally, though it remains a challenge to get the location of the auroral boundary for this storm, it must be emphasized that the boundary could have been located much further south of the US/Mexico boarder based on reported aurora sightings.

Data availability statement

Solar wind measurements were obtained from the NASA/GSFC Space Physics Data Facility OMNIWeb service produced by CDAWeb at https://omniweb.gsfc.nasa.gov/. The SuperMag data is collected at ground magnetometer stations around the world and made available at http://supermag.jhuapl.edu/. Ionospheric currents were derived using the SECS technique at 10 s Resolution in Geographic Coordinates (Weygand, 2009a), whereas the SEC Amplitudes were also derived using the SECS technique at 10 s Resolution in Geographic Coordinates (Weygand, 2009b).

Author contributions

CN: Writing – review and editing, Software, Writing – original draft, Validation, Funding acquisition, Resources, Investigation, Project administration, Formal Analysis, Conceptualization, Methodology, Data curation, Visualization. YN: Validation, Methodology, Conceptualization, Visualization, Investigation, Data curation, Funding acquisition, Writing – review and editing, Formal Analysis. JW: Formal Analysis, Methodology, Data curation, Visualization, Validation, Conceptualization, Funding acquisition, Writing – original draft, Writing – review and editing, Investigation. LL: Resources, Data curation, Writing – review and editing. DB: Visualization, Resources, Writing – review and editing. JF: Writing – review and editing, Investigation, Resources, Formal Analysis. PE: Writing – review and editing, Resources, Formal Analysis.

Funding

The author(s) declare that financial support was received for the research and/or publication of this article. This work was partly supported by NASA Grant Award 80NSSC24K0259. CMN was also supported by NSF Grant Award AGS-2300579. YN was also supported by NASA grants 80NSSC21K1321, 80NSSC23M0193, 80NSSC23K0410, 80NSSC24K1103, and 80NSSC25K0075, NSF grant AGS-2527835, and AFOSR grant FA9550-23-1-0614. JF, PJE, and DCB received no financial support for work on this study.

Acknowledgments

For the ground magnetometer data we gratefully acknowledge: INTERMAGNET, Alan Thomson; CARISMA, PI Ian Mann; CANMOS, Geomagnetism Unit of the Geological Survey of Canada; The S-RAMP Database, PI K. Yumoto and Dr. K. Shiokawa; The SPIDR database; AARI, PI Oleg Troshichev; The MACCS program, PI M. Engebretson; GIMA; MEASURE, UCLA IGPP and Florida Institute of Technology; SAMBA, PI Eftyhia Zesta; 210 Chain, PI K. Yumoto; SAMNET, PI Farideh Honary; IMAGE, PI Liisa Juusola; Finnish Meteorological Institute, PI Liisa Juusola; Sodankylä Geophysical Observatory, PI Tero Raita; UiT the Arctic University of Norway, Tromsø Geophysical Observatory, PI Magnar G. Johnsen; GFZ German Research Centre For Geosciences, PI Jürgen Matzka; Institute of Geophysics, Polish Academy of Sciences, PI Anne Neska and Jan Reda; Polar Geophysical Institute, PI Alexander Yahnin and Yarolav Sakharov; Geological Survey of Sweden, PI Gerhard Schwarz; Swedish Institute of Space Physics, PI Masatoshi Yamauchi; AUTUMN, PI Martin Connors; DTU Space, Thom Edwards and PI Anna Willer; South Pole and McMurdo Magnetometer, PI's Louis J. Lanzarotti and Alan T. Weatherwax; ICESTAR; RAPIDMAG; British Artarctic Survey; McMac, PI Dr. Peter Chi; BGS, PI Dr. Susan Macmillan; Pushkov Institute of Terrestrial Magnetism, Ionosphere and Radio Wave Propagation (IZMIRAN); MFGI, PI B. Heilig; University of L'Aquila, PI M. Vellante; BCMT, V. Lesur and A. Chambodut; Data obtained in cooperation with Geoscience Australia, PI Andrew Lewis; PENGUIn, co-PIs Bob Clauer, Michael Hartinger, and Zhonghua Xu; MagStar, PI Jennifer Gannon; LISN PI Cesar Valladares; SuperMAG, PI Jesper W. Gjerloev; Data obtained in cooperation with the Australian Bureau of Meteorology, PI Richard Marshall. SuperMAG is funded by NSF, NASA, and ESA.

Conflict of interest

The authors declare that the research was conducted in the absence of any commercial or financial relationships that could be construed as a potential conflict of interest.

Generative AI statement

The author(s) declare that no Generative AI was used in the creation of this manuscript.

Any alternative text (alt text) provided alongside figures in this article has been generated by Frontiers with the support of artificial intelligence and reasonable efforts have been made to ensure accuracy, including review by the authors wherever possible. If you identify any issues, please contact us.

Publisher's note

All claims expressed in this article are solely those of the authors and do not necessarily represent those of their affiliated organizations, or those of the publisher, the editors and the reviewers. Any product that may be evaluated in this article, or claim that may be made by its manufacturer, is not guaranteed or endorsed by the publisher.

References

Amm, O. (1997). Ionospheric elementary current systems in spherical coordinates and their application. *J. Geomagnetism Geoelectr.* 49, 947–955. doi:10.5636/jgg.49.947

Amm, O., Engebretson, M. J., Hughes, T., Newitt, L., Viljanen, A., and Watermann, J. (2002). A traveling convection vortex event study: instantaneous ionospheric equivalent currents, estimation of field-aligned currents, and the role of induced currents. *J. Geophys. Res.* 107, SIA1–SIA11. doi:10.1029/2002JA009472

Anderson, B. J., Korth, H., Waters, C. L., Green, D. L., and Stauning, P. (2008). Statistical Birkeland current distributions from magnetic field observations by the Iridium constellation. *Ann. Geophys.* 26, 671–687. doi:10.5194/angeo-26-671-2008

Boteler, D. H. (2019). A 21st century view of the March 1989 magnetic storm. *Space weather.* 17, 1427–1441. doi:10.1029/2019SW002278

Chu, X., McPherron, R. L., Hsu, T. S., and Angelopoulos, V. (2015). Solar cycle dependence of substorm occurrence and duration: implications for onset. *J. Geophys. Res.* 120, 2808–2818. doi:10.1002/2015JA021104

Despirak, I., Kozelova, T., Koselov, B., and Lubchich, A. (2022). "Observations of substorm activity near the Harang Discontinuity," in *Eighteenth international scientific conference "space, ecology, safety" (SES-2022)* (Sofia, Bulgaria), 19–21.

Engebretson, M. J., Simms, L. E., Pilipenko, V. A., Bouayed, L., Moldwin, M. B., Weygand, J. M., et al. (2022). Geomagnetic disturbances that cause GICs: investigating their interhemispheric conjugacy and control by IMF orientation. *J. Geophys. Res.* 127, e2022JA030580. doi:10.1029/2022JA030580

Engebretson, M. J., Gaffaney, S. A., Ochoa, J. A., Runov, A., Weygand, J. M., Nishimura, Y., et al. (2024). Signatures of dipolarizing flux bundles in the nightside auroral zone. *J. Geophys. Res.* 129, e2023JA032266. doi:10.1029/2023JA032266

Erickson, G. M., Spiro, R. W., and Wolf, R. A. (1991). The physics of the Harang discontinuity. *J. Geophys. Res.* 96 (A2), 1633–1645. doi:10.1029/90ja02344

Forsythe, V. V., Duly, T., Hampton, D., and Nguyen, V. (2020). Validation of ionospheric electron density measurements derived from Spire CubeSat constellation. *Radio Sci.* 55, e2019RS006953. doi:10.1029/2019RS006953

Foster, J. C., Erickson, P. J., Nishimura, Y., Zhang, S. R., Bush, D. C., Coster, A. J., et al. (2024). Imaging the may 2024 extreme aurora with ionospheric total electron content. *Geophys. Res. Lett.* 51, e2024GL111981. doi:10.1029/2024GL111981

Gaunt, C. T., and Coetzee, G. (2007). "Transformer failure in regions incorrectly considered to have low gic-risks," in *IEEE power tech., conference paper 445* (Lausanne), 807–812.

Gjerloev, J. W. (2009). A global ground-based magnetometer initiative. *Eos* 90, 230–231. doi:10.1029/2009EO270002

Gonzalez-Esparza, J. A., Sanchez-Garcia, E., Sergeeva, M., Corona-Romero, P., Gonzalez-Mendez, L. X., Valdes-Galicia, J. F., et al. (2024). The mother's day geomagnetic storm on 10 may 2024: aurora observations and low latitude space weather effects in Mexico. *Space weather.* 22, e2024SW004111. doi:10.1029/2024SW004111

Grocott, A., Milan, S. E., Yeoman, T. K., Sato, N., Yukimatu, A. S., and Wild, J. A. (2010). Superposed epoch analysis of the ionospheric convection evolution during substorms: IMF B_Y dependence. *J. Geophys. Res.* 115. doi:10.1029/2010JA015728

Hajra, R., Tsurutani, B. T., Echer, E., Gjerlov, J. W., and Gjerloev, J. W. (2016). Supersubstorms (SML < −−2500 nT): magnetic storm and solar cycle dependences. *Geophys. Res. Lett.* 121, 7805–7816. doi:10.1002/2015JA021835

Harang, L. (1946). The mean field of disturbance of polar geomagnetic storms. *Terr. Magnetism Atmos. Electr.* 51 (3), 353–380. doi:10.1029/te051i003p00353

Hayakawa, H., Ebihara, Y., Mishev, A., Koldobskiy, S., Kusano, K., Bechet, S., et al. (2025). The solar and geomagnetic storms in 2024 may: a flash data report. *Astrophysical J.* 979, 49. doi:10.3847/1538-4357/ad9335

Henderson, M. G., Reeves, G. D., and Murphree, J. S. (1998). Are north-south aligned auroral structures an ionospheric manifestation of bursty bulk flows? *Geophys. Res. Lett.* 25 (19), 3737–3740. doi:10.1029/98gl02692

Holappa, L., Robinson, R. M., Pulkkinen, A., Asikainen, T., and Mursula, K. (2021). Explicit IMF b_y-dependence in geomagnetic activity: quantifying ionospheric electrodynamics. *J. Geophys. Res.* 126, e2021JA029202. doi:10.1029/2021JA029202

Kleimenova, N., Gromova, L., Gromov, S., and Malysheva, L. (2025). Ground-based geomagnetic disturbances and pi2 pulsations in the main phase of the superstorm on may 10, 2024. *Adv. Space Res.* doi:10.1016/j.asr.2025.04.025

Lao, C. J., Forsyth, C., Freeman, M. P., Smith, A. W., and Mooney, M. K. (2024). On the association of substorm identification methods. *J. Geophys. Res. - Space Phys.* 129, e2024JA032762. doi:10.1029/2024JA032762

Lyons, L. R., Nishimura, Y., Kim, H.-J., Donovan, E., Angelopoulos, V., Sofko, G., et al. (2011). Possible connection of polar cap flows to pre- and post-substorm onset PBIs and streamers. *J. Geophys. Res.* 116. doi:10.1029/2011JA016850

Lyons, L. R., Nishimura, Y., Donovan, E., and Angelopoulos, V. (2013). Distinction between auroral substorm onset and traditional ground magnetic onset signatures. *J. Geophys. Res.* 118, 4080–4092. doi:10.1002/jgra.50384

Maynard, N. C. (1974). Electric field measurements across the Harang discontinuity. *J. Geophys. Res.* 79, 4620–4631. doi:10.1029/JA079i031p04620

McPherron, R. L., and Chu, X. (2017). The mid-latitude positive bay and the MPB index of substorm activity. *Space Sci. Rev.* 206, 91–122. doi:10.1007/s11214-016-0316-6

Milan, S. E., Mooney, M. K., Bower, G., Fleetham, A. L., Vines, S. K., and Gjerloev, J. (2023). Solar wind-magnetosphere coupling during high-intensity long-duration continuous AE activity (HILDCAA). *Geophys. Res. Lett.* 128, e2023JA032027. doi:10.1029/2023JA032027

Milan, S. E., Bower, G. E., Fleetham, A. L., Imber, S. M., Schillings, A., Opgenoorth, H., et al. (2024). Occurrence and causes of large *dB*/*dt* events and AL bays in the pre-midnight and dawn sectors. *Geophys. Res. Lett.* 129, e2024JA032811. doi:10.1029/2024JA032811

Newell, P. T., and Gjerloev, J. G. (2011). Evaluation of SuperMAG auroral electrojet indices as indicators of substorms and auroral power. *J. Geophys. Res.* 116, A12211. doi:10.1029/2011JA016779

Ngwira, C. M., Pulkkinen, A., Wilder, F. D., and Crowley, G. (2013). Extended study of extreme geoelectric field event scenarios for geomagnetically induced current applications. *Space weather.* 11, 121–131. doi:10.1002/swe.20021

Ngwira, C. M., Pulkkinen, A., Bernabeu, E., Eichner, J., Viljanen, A., and Crowley, G. (2015). Characteristics of extreme geoelectric fields and their possible causes: localized peak enhancements. *Geophys. Res. Lett.* 42, 6916–6921. doi:10.1002/2015GL065061

Ngwira, C. M., Sibeck, D., Silveria, M. V. D., Georgiou, M., Weygand, J. M., Nishimura, Y., et al. (2018). A study of intense local dB/dt variations during two geomagnetic storms. *Space weather.* 16, 676–693. doi:10.1029/2018SW001911

Ngwira, C. M., Arritt, R., Perry, C., Weygand, J. M., and Rishi, S. (2023). Occurrence of large geomagnetically induced currents within the EPRI SUNBURST monitoring network. *Space weather.* 21 (12), e2023SW003532. doi:10.1029/2023SW003532

Ngwira, C. M., Nishimura, Y., Weygand, J. M., Engebretson, M. J., Pulkkinnen, A., and Schuck, P. (2025). Observations of localized horizontal geomagnetic field variations associated with a magnetospheric fast flow burst during a magnetotail reconnection event detected by the THEMIS spacecraft. *J. Geophys. Res. Space Phys.* 130, e2024JA032651. doi:10.1029/2024JA032651

North American Electric Reliability Corporation (1989). *NERC hydro quebec GMD event report*.

Ohtani, S., and Gjerloev, J. W. (2020). Is the substorm current wedge an ensemble of wedgelets? Revisit to midlatitude positive bays. *J. Geophys. Res.* 125, e2020JA027902. doi:10.1029/2020JA027902

Ohtani, S., Gjerloev, J. W., Anderson, B. J., Kataoka, R., Troshichev, O., and Watari, S. (2018). Dawnside wedge current system formed during intense geomagnetic storms. *J. Geophys. Res.* 123, 9093–9109. doi:10.1029/2018JA025678

Ohtani, S., Sorathia, K., Merkin, S. G., Frey, H. U., and Gjerloev, J. W. (2023). External and internal causes of the stormtime intensification of the dawnside westward auroral electrojet. *J. Geophys. Res.* 128 (10), e2023JA031457. doi:10.1029/2023JA031457

Ohtani, S., Zou, Y., Merkin, V. G., Wiltberger, M., Pham, K. H., Raptis, S., et al. (2025). Ground magnetic response to an extraordinary IMF B_Y flip during the may 2024 storm: travel time from the magnetosheath to dayside high latitudes. *J. Geophys. Res.* 130, e2024JA033691. doi:10.1029/2024JA033691

Opgenoorth, H. J., Robinson, R., Ngwira, C. M., Garcia Sage, K., Kuznetsova, M., El Alaoui, M., et al. (2024). Earth's geomagnetic environment–progress and gaps in understanding, prediction, and impacts. *Adv. Space Res.* doi:10.1016/j.asr.2024.05.016

Piersanti, M., Oliveira, D. M., D'Angelo, G., Diego, P., Napoletano, G., and Zesta, E. (2025). On the geoelectric field response to the SSC of the may 2024 super storm over europe. *Space weather.* 23, e2024SW004191. doi:10.1029/2024SW004191

Pirjola, R. (2000). Geomagnetically induced currents during magnetic storms. *IEEE Trans. Plasma Sci.* 28, 1867–1873. doi:10.1109/27.902215

Pulkkinen, A., Bernabeu, E., Eichner, J., Beggan, C., and Thomson, A. W. P. (2012). Generation of 100-year geomagnetically induced current scenarios. *Space weather.* 10, S04003. doi:10.1029/2011SW000750

Pulkkinen, A., Bernabeu, E., Thomson, A., Viljanen, A., Pirjola, R., Boteler, D., et al. (2017). Geomagnetically induced currents: science, engineering and applications readiness. *Space weather.* 15, 828–856. doi:10.1002/2016SW001501

Sorathia, K. A., Michael, A., Merkin, V. G., Ohtani, S., Keesee, A. M., Sciola, A., et al. (2023). Multiscale magnetosphere-ionosphere coupling during stormtime: a case study of the dawnside current wedge. *J. Geophys. Res.* 128, e2023JA031594. doi:10.1029/2023JA031594

Tsurutani, B. T., Hajra, R., Echer, E., and Gjerloev, J. W. (2015). Extremely intense (SML ≤−2500 nT) substorms: isolated events that are externally triggered? *Ann. Geophys.* 33, 519–524. doi:10.5194/angeo-33-519-2015

Tulasi Ram, S., Veenadhari, B., Dimri, A. P., Bulusu, J., Bagiya, M., Gurubaran, S., et al. (2024). Super–intense geomagnetic storm on 10–11 may 2024: possible mechanisms and impacts. *Space weather.* 22, e2024SW004126. doi:10.1029/2024SW004126

Vichare, G., and Bagiya, M. S. (2024). Manifestations of strong imf-by on the equatorial ionospheric electrodynamics during 10 may 2024 geomagnetic storm. *Geophys. Res. Lett.* 51, e2024GL112569. doi:10.1029/2024GL112569

Waghule, B., and Knipp, D. J. (2025). *Ionospheric response during the 10–12 may 2024 geomagnetic storm and it's connection to GICs. 2025 United States national committee of URSI national Radio science meeting*. Boulder, CO, USA: USNC-URSI NRSM, 362–363. doi:10.23919/USNC-URSINRSM66067.2025.10906842

Waghule, B., Knipp, D. J., Gannon, J. L., Billet, D., Vines, S. K., and Goldstein, J. (2024). What drove the GICs >10 A during the 17 March 2013 event at Mäntsälä? *Space weather.* 22, e2024SW003980. doi:10.1029/2024SW003980

Wei, D., Dunlop, M. W., Yang, J., Dong, X., Yu, Y., and Wang, T. (2021). Intense dB/dt variations driven by near-earth bursty bulk flows (BBFs): a case study. *Geophys. Res. Lett.* 48, e2020GL091781. doi:10.1029/2020GL091781

Weygand, J. M. (2009a). *Spherical elementary currents systems (SECS) technique North American equivalent ionospheric currents (EICs) derived at 10 sec resolution in geographic coordinates*. Los Angeles: University of California. doi:10.21978/p8d62b

Weygand, J. M. (2009b). *Spherical elementary currents systems (SECS) technique North American spherical elementary current (SEC) amplitudes derived at 10 sec resolution in geographic coordinates [data set]*. Los Angeles: University of California. doi:10.21978/p8pp8x

Weygand, J. M., McPherron, R. L., Frey, H., Amm, O., Kauristie, K., Viljanen, A. T., et al. (2008). Relation of substorm onset to Harang discontinuity. *J. Geophys. Res.* 113, A04213. doi:10.1029/2007JA012537

Weygand, J. M., Amm, O., Viljanen, A., Angelopoulos, V., Murr, D., Engebretson, M. J., et al. (2011). Application and validation of the spherical elementary currents systems technique for deriving ionospheric equivalent currents with the North American and Greenland ground magnetometer arrays. *J. Geophys. Res.* 116, A03305. doi:10.1029/2010JA016177

Weygand, J. M., Amm, O., Angelopoulos, V., Milan, S. E., Grocott, A., Gleisner, H., et al. (2012). Comparison between SuperDARN flow vectors and equivalent ionospheric currents from ground magnetometer arrays. *J. Geophys. Res.* 117, A05325. doi:10.1029/2011JA017407

Weygand, J. M., Ngwira, C. M., and Arritt, R. F. (2023). The equatorward boundary of the auroral current system during magnetic storms. *J. Geophys. Res.* 128, e2023JA031510. doi:10.1029/2023JA031510

Wik, M., Pirjola, R., Lundstedt, H., Viljanen, A., Wintoft, P., and Pulkkinen, A. (2009). Space Weather events in July 1982 and October 2003 and the effects of geomagnetically induced currents on Swedish technical systems. *Ann. Geophys.* 27, 1775–1787. doi:10.5194/angeo-27-1775-2009

Yoshizawa, K. (1986). Effect of the IMF-By component on the North–South asymmetry of geomagnetic activity. *Planet. Space Sci.* 34, 639–644. doi:10.1016/0032-0633(86)90041-3

Zhang, Z., Zhang, F., Wang, L., Li, X., Zhima, Z., Wang, Y., et al. (2025). The magnetosphere–ionosphere–ground responses to the May 2024 super solar storm. *Space weather.* 23, e2024SW004197. doi:10.1029/2024SW004197

Zou, S., Lyons, L. R., Wang, C.-P., Boudouridis, A., uohoniemi, J. M., Dyson, P. C. A. P. L., et al. (2009). On the coupling between the Harang reversal evolution and substorm dynamics: a synthesis of SuperDARN, DMSP, and IMAGE observations. *J. Geophys. Res.* 114. doi:10.1029/2008JA013449

Zou, Y., Dowell, C., Ferdousi, B., Lyons, L. R., and Liu, J. (2022). Auroral drivers of large dB/dt during geomagnetic storms. *Space weather.* 20, e2022SW003121. doi:10.1029/2022SW003121

Zou, Y., Shin, O., Gjerloev, J. W., Anderson, B. J., Waters, C. L., Wang, C.-P., et al. (2025). Are supersubstorms substorms? Extreme nightside auroral electrojet activities during the may 2024 geomagnetic storm. *J. Geophys. Res. Space Phys.* 130, e2024JA033303. doi:10.1029/2024JA033303